Chapter IV

Velocity Stack Generalized Inverses

4.1 The problem

The previous chapter presented the main features of pseudoinverse theory for slant stack operators. A linear transformation more appropriate for use on seismic data, in particular common-midpoint gathers (CMGs), is normal moveout and stacking. For example, one of the two most common methods used to determine average velocities from a CMG is to perform a velocity stack; i.e., to sum the CMG over hyperbolic paths corresponding to a set of velocities. Peaks in the velocity panel are a result of constructively summing a reflection along the moveout corresponding to its average velocity. The other, more common way to determine average velocities is to replace the summation with a semblance measure; however, this method is a nonlinear one, because semblance measures involve products of the gather's elements (Douze and Laster, 1979). In this chapter we shall restrict ourselves to the linear operation of velocity stacking, and address the same questions to the velocity stack that were answered in chapter 3 with respect to the slant stack: namely the questions of invertibility and the nature of the generalized inverse.

Recall that velocity stacking was defined in chapter 2 by equation (2.30), one of a pair of mutually adjoint linear transformations L, L^T:

$\mathbf{L}$: $$d(h,t) = \int_0^\infty dp\ u(p, \sqrt{t^2 - p^2h^2}) \tag{2.29}$$

$\mathbf{L}^T$: $$u(p,\tau) = \int_0^\infty dh\ d(h, \sqrt{\tau^2 + p^2h^2}) \tag{2.30}$$

It must be emphasized that in order for these symmetric definitions of $\mathbf{L}$ and $\mathbf{L}^T$ to be mutually adjoint, the inner products in both offset and velocity space must be defined with a linear weighting in time (equations 2.24 and 2.25). If $(\mathbf{u}, \tilde{\mathbf{u}})_V$ denotes the inner product of two functions $u(p,\tau)$ and $\tilde{u}(p,\tau)$ in velocity (V) space (a similar notation is made for the inner product in offset (H) space), the relationship that defines the adjoint operator is

$$(\mathbf{u}, \mathbf{L}^T\mathbf{d})_V = (\mathbf{d}, \mathbf{L}\mathbf{u})_H \tag{4.1}$$

The following discussion will involve those versions of the velocity stack operators that have finite limits in velocity and offset:

$\mathbf{P_d L}$: $$d(h,t) = \int_{p_1}^{p_2} dp\ u(p, \sqrt{t^2 - p^2h^2}) \tag{4.2}$$

$\mathbf{L}^T\mathbf{P_d}$: $$u(p,\tau) = \int_{h_1}^{h_2} dh\ d(h, \sqrt{\tau^2 + p^2h^2}) \tag{4.3}$$

As was done in chapter 2, these truncations may be incorporated into the projectors $\mathbf{P}_u$ and $\mathbf{P}_d$. Furthermore all slownesses and offsets considered within range will be positive:

$$P_u(p,\tau) = \begin{cases} 1 & 0 \le p_1 \le p \le p_2 < \infty \\ 0 & \text{otherwise} \end{cases} \tag{4.4}$$

$$P_d(h,t) = \begin{cases} 1 & 0 \le h_1 \le h \le h_2 < \infty \\ 0 & \text{otherwise} \end{cases} \tag{4.5}$$

In this chapter we shall be concerned with solving the so-called "type I" problem of section 2.6: solving for $\mathbf{u}$ in the equation

$$\mathbf{d} = \mathbf{P_d L P_u u} + \mathbf{n} \tag{2.32}$$

In chapter 3, a reasonable constraint was imposed on the solution **u**: it is nonzero only between slowness limits p_1 and p_2 (equation 3.3). We shall make the same assumption here so that the term $\mathbf{P}_u$ need not be carried about in the equations; it will be incorporated into L.

Recall that the generalized inverse solution to the type I problem is

$$\mathbf{u} = (\mathbf{L}^T\mathbf{P}_d\mathbf{L})^+\mathbf{L}^T\mathbf{P}_d\mathbf{d} \tag{4.6}$$

Let us now follow a development similar to that of chapter 3, to derive the filter $(\mathbf{L}^T\mathbf{P}_d\mathbf{L})^+$. Unfortunately we will run into some snags along the way, but with the aid of the theorem of section 2.7, these problems may be overcome. Later in the chapter, we will illustrate the application of the generalized inverse filter to both synthetic and real data sets. The example of figure 1.2 was generated using the generalized filter derived here.

4.2 The impulse response of $\mathbf{L}^T\mathbf{P}_d\mathbf{L}$

The first step in deriving the generalized inverse is to find the impulse response of $\mathbf{L}^T\mathbf{P}_d\mathbf{L}$. From equation (4.2), the response $\mathbf{L}\delta$ to an impulse $\delta(p-\tilde{p})\delta(\tau-\tilde{\tau})$ at $p = \tilde{p}$, $\tau = \tilde{\tau}$ is

$$\begin{aligned} d(h,t) &= \delta(\sqrt{t^2 - \tilde{p}^2h^2} - \tilde{\tau}) \\ &= \frac{\tilde{\tau}}{t}\delta(t - \sqrt{\tilde{\tau}^2 + \tilde{p}^2h^2}) \end{aligned} \tag{4.7}$$

Here we use a theorem on changing variables in a Dirac delta distribution (Bracewell, 1965, p. 95) which states that

$$\delta(f(x)) = \sum_j \frac{\delta(x - x_j)}{|f'(x_j)|} \tag{4.8}$$

where x_j are all the roots of $f(x)$: $f(x_j) = 0$. If the range of the integral containing $\delta(f(x))$ is restricted to exclude some roots x_j, these terms will not be included in the sum of equation (4.8). Likewise, when $\tilde{p}$ is outside the range of (p_1, p_2) the

response $d(h,t)$ is obviously zero. The impulse response $\mathbf{L}^T\mathbf{P}_d\mathbf{L}\delta$ is found by applying $\mathbf{L}^T\mathbf{P}_d$ (equation 4.3) to $\mathbf{L}\delta$ (equation 4.7):

$$u(p,\tau) = \int_{h_1}^{h_2} dh \; \frac{\tilde{\tau}}{\tilde{t}}\delta(t - \tilde{t}) \qquad \begin{cases} t \equiv \sqrt{\tau^2 + p^2h^2} \\ \tilde{t} \equiv \sqrt{\tilde{\tau}^2 + \tilde{p}^2h^2} \end{cases} \tag{4.9}$$

The delta function $\delta(t - \tilde{t})$ is nonzero for a unique offset $h^2 = h_0^2$, and can be transformed into a delta function in h in order that the sifting property of the Dirac delta distribution may be used:

$$u(p,\tau) = \int_{h_1}^{h_2} dh \; \frac{\tilde{\tau}\;\; t \;\; \delta(h - h_0)}{\tilde{t}\; h_0 \; |p^2 - \tilde{p}^2|} \tag{4.10}$$

where

$$h_0 \equiv -\frac{\tau^2 - \tilde{\tau}^2}{p^2 - \tilde{p}^2} \tag{4.11}$$

Now at $h = h_0$, $\tilde{t}$ is equal to t. The sifting property allows us to set u equal to the integrand, except when h_0 falls outside the range of (h_1, h_2). When this occurs, $u(p,\tau)$ is identically equal to zero. Taking this fact into account, and substituting for h_0 , the impulse response $\mathbf{L}^T\mathbf{P}_d\mathbf{L}\delta$ from equation (4.10) becomes:

$$u(p,\tau) = \tilde{\tau}\frac{H\left(h_0 - h_1^2\right)H\left(h_2^2 - h_0\right)}{|p^2 - \tilde{p}^2|^{1/2}\,|\tau^2 - \tilde{\tau}^2|^{1/2}} \tag{4.12}$$

where $H(x)$ is the unit step function. The nonzero parts of the filter are bounded by the curves $h_0 = h_1^2$ and $h_0 = h_2^2$, which pass through the origin; h_0 is the function of p and τ given in equation (4.11).

Using the impulse response of equation (4.12), we can write the transformation $\mathbf{L}^T\mathbf{P}_d\mathbf{L}$ in integral form:

$$u(p,\tau) = \int_0^\infty\!\!\int d\tilde{p}\; d\tilde{\tau}\; \tilde{\tau}\; K(p^2 - \tilde{p}^2,\, \tau^2 - \tilde{\tau}^2)\; \tilde{u}(\tilde{p},\tilde{\tau}) \tag{4.13}$$

where the kernel K is

$$K(x,y) = |xy|^{-1/2} H\left(-\frac{y}{x} - h_1^2\right) H\left(h_2^2 - \frac{y}{x}\right) \tag{4.14}$$

The kernel is illustrated in figure 4.1.

4.3 The generalized inverse in the p^2, τ^2 domain

The next step, as it was in the case of slant stacking, is to get the kernel of $\mathbf{L}^T\mathbf{P}_d\mathbf{L}$ in convolutional form, in order that the kernel of the generalized inverse may be determined in Fourier space. The kernel is non-convolutional in p and τ, but apart from the factor $\tilde{\tau}$, can be made convolutional by the obvious transformation to independent variables $x = p^2$ and $y = \tau^2$. This is the only practical way that the generalized inverse can be determined. This change of variables transforms equation (4.13) into

$$u(x^{1/2}, y^{1/2}) = \int_0^\infty\int \frac{d\tilde{x}}{2\tilde{p}} \frac{d\tilde{y}}{2\tilde{\tau}} \tilde{\tau}\, K(x-\tilde{x}, y-\tilde{y})\, \tilde{u}(\tilde{x}^{1/2}, \tilde{y}^{1/2}) \tag{4.15}$$

The Fourier transform of the kernel K in equation (4.14) turns out to have a simple expression:

$$\begin{aligned}\tilde{K}(\xi,\eta) &= \int_{-\infty}^{\infty}\int dx\, dy\, |xy|^{-1/2} H\left(-\frac{y}{x} - h_1^2\right) H\left(h_2^2 + \frac{y}{x}\right) e^{-i\xi x - i\eta y} \\ &= 2\pi |\xi\eta|^{-1/2} H\left(\frac{\xi}{\eta} - h_1^2\right) H\left(h_2^2 - \frac{\xi}{\eta}\right)\end{aligned} \tag{4.16}$$

The symmetric definition (3.13) of the Fourier transform has been used. Recall that the extra 2π factor results from using equation (3.18), the rule for transforming convolutional kernels into the Fourier domain. The generalized inverse is defined to be the inverse of the nonzero region of the filter.

$$\tilde{K}^+(\xi,\eta) \equiv \frac{1}{2\pi} |\xi\eta|^{1/2} H\left(\frac{\xi}{\eta} - h_1^2\right) H\left(h_2^2 - \frac{\xi}{\eta}\right) \tag{4.17}$$

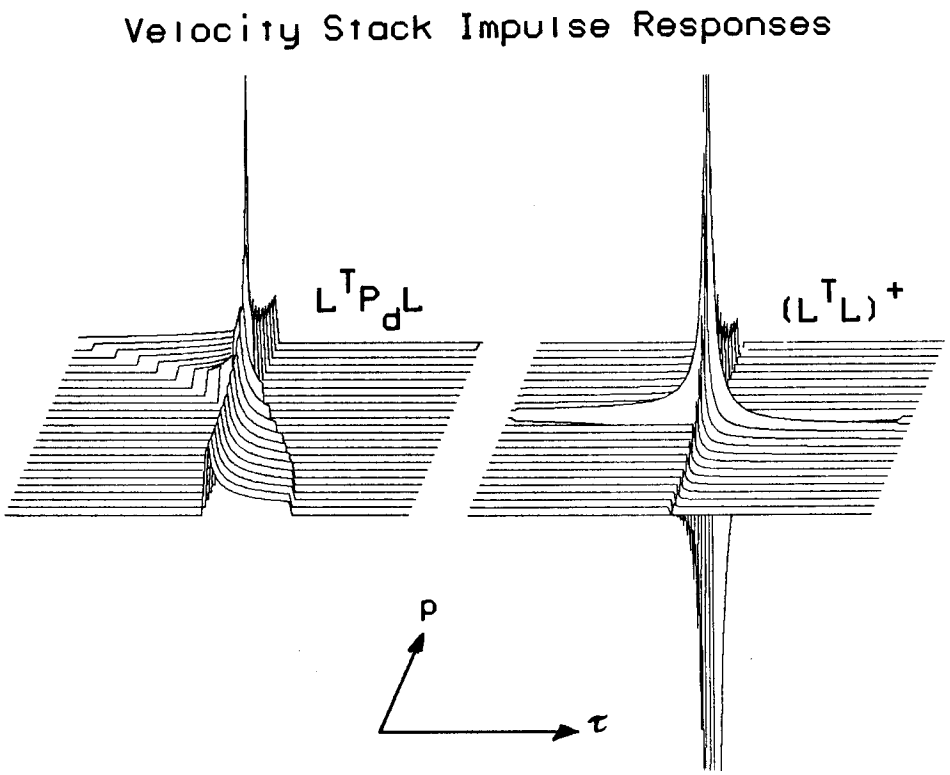

FIG. 4.1. Velocity stacking impulse responses. The left panel is the response $\mathbf{L}^T\mathbf{P}_d\mathbf{L}\boldsymbol{\delta}$ to an impulse centered in the p,τ plane shown. The curved truncation edge is due to the unit step terms in equation (4.12). Considered as a two-dimensional filter, it is not stationary: it varies both in time (τ) and slowness (p).

The right panel is the generalized inverse $(\mathbf{L}^T\mathbf{L})^+$, derived in section 4.3; the offset limits used in its derivation were $(h_1, h_2) = (0, \infty)$, respectively. It is a p- and τ-variable filter. The filter is strictly positive in quadrants II and IV of the p, τ plane; zero in the other two quadrants; has large negative values on both axes, and an even greater positive value at the origin. Because the sign of the filter changes upon crossing the p, τ axes, the generalized inverse acts very much like a differentiator in both p and τ.

The inverse Fourier transform to (4.17) is derived in appendix 4.A, and is, for $(x,y) \neq (0,0)$,

$$
\begin{aligned}
K^+(x,y) \;=\; & \frac{1}{16\pi^2}|xy|^{-3/2}\, H\!\left(-\frac{y}{x} - h_1^2\right) H\!\left(h_2^2 + \frac{y}{x}\right) \\
& - \frac{1}{8\pi^2}|x|^{-3/2}|y|^{-1/2}\left(\delta(y + h_2^2 x) - \delta(y + h_1^2 x)\right) \\
& + \frac{1}{4\pi^2}|xy|^{-1/2}\operatorname{sgn}(y)\left(\delta'(y + h_2^2 x) - \delta'(y + h_1^2 x)\right) \qquad (4.18)
\end{aligned}
$$

Though it looks rather formidable, this filter can be easily described. It is restricted to be nonzero between the "edges" of the filter: the curves $y = -h_1^2 x$ and $y = -h_2^2 x$. In the interior of this region the filter coefficients are given by the first term, $|xy|^{-3/2}/16\pi^2$. The two remaining terms contain deltas and delta derivatives, and apply only at the edges of the filter. These edge terms can be considered as necessary to satisfy the various zero-DC-component constraints imposed by the Fourier-space version of the filter. These constraints are

$$\tilde{K}^+(\xi,\eta) = 0 \quad \text{for } \xi=0 \qquad \int_{-\infty}^{\infty} dx\ K^+(x,y) = 0 \quad \text{for all } y$$

$$\tilde{K}^+(\xi,\eta) = 0 \quad \text{for } \eta=0 \qquad \int_{-\infty}^{\infty} dy\ K^+(x,y) = 0 \quad \text{for all } x \qquad (4.19)$$

It is not clear what $K^+(x,y)$ should reduce to as the aperture is widened to the largest possible range of offsets, $h_1 \to 0$ and $h_2 \to \infty$. But regardless of the aperture, the constraints in equation (4.19) still apply. They may be used to determine the coefficients on the x axis ($h_1 = 0$), the y axis ($h_2 = \infty$), and at the origin in a discrete implementation of the full aperture filter. For example, the interior of the filter lies in quadrants II and IV of the x,y plane, and is proportional to $|xy|^{-3/2}$. To satisfy constraints (4.19), coefficients on the x and y axes must be large negative numbers (in the continuous case they are proportional to $|\varepsilon|^{-1/2}\delta(\varepsilon)$ as $\varepsilon \to 0$). Finally, the value at the origin must be an even larger positive value, to guarantee that the filter has no overall DC component.

The kernel can be brought back into the p,τ domain by a change of variables (compare this to equation 4.15):

$$\frac{u(x^{1/2}, y^{1/2})}{4p} = \iint_0^\infty K^+(x - \tilde{x}, y - \tilde{y})\, \tilde{u}(\tilde{x}^{1/2}, \tilde{y}^{1/2})\, d\tilde{x}\, d\tilde{y} \qquad (4.20)$$

$$u(x, y) = \iint_0^\infty 16p\tilde{p}\tilde{\tau}\, K^+(p^2 - \tilde{p}^2, \tau^2 - \tilde{\tau}^2)\, \tilde{u}(\tilde{p}, \tilde{\tau})\, d\tilde{p}\, d\tilde{\tau} \qquad (4.21)$$

The various kernels in p,τ space are summarized in table 4.1. The infinite-aperture impulse response of the generalized inverse $(\mathbf{L}^T\mathbf{L})^+$ is also illustrated in figure 4.1.

4.4 Infinite-aperture versus finite-aperture filters

The filter $(\mathbf{L}^T\mathbf{P}_d\mathbf{L})^+$ derived in the last section is not a generalized inverse in the strict sense defined in chapter 2, because it was necessary to perform a τ^2, p^2 mapping before the Fourier transform could be taken. Nevertheless it is a true generalized inverse in the remapped domain. Let us now put this filter in the operator notation of section 2.7, and address the following questions. What is the relationship between the inverses of table 4.1 and the slant stack inverses of table 3.1? Does the theorem of section 2.7 hold, so that $(\mathbf{L}^T\mathbf{L})^+$ may be used in place of $(\mathbf{L}^T\mathbf{P}_d\mathbf{L})^+$ in practice?

The generalized inverse was derived by the following steps: change variables, transform the kernel to the Fourier domain; invert the nonzero singular values; inverse transform; and undo the change of variables. Each of these steps is linear. The change of variables $x = p^2$, $y = \tau^2$ is an invertible linear transformation **S**, and is necessary to allow the diagonalization of the operator by the (unitary) Fourier transform:

$$\mathbf{L}^T\mathbf{P}_d\mathbf{L}\mathbf{u} = \mathbf{S}^{-1}\mathbf{U}\Sigma^2\mathbf{U}^T\mathbf{S}\mathbf{W}\mathbf{u} \qquad (4.22)$$

$\mathbf{U}^T$ is the forward Fourier transform. Σ^2 is diagonal (multiplicative); it consists of the values of the Fourier-transformed kernel given by equation (4.16). There is an additional diagonal weighting **W**, which represents the prescaling of $\tilde{u}$ by $1/4\tilde{p}$ in equation (4.20). According to strict definition, this decomposition of $\mathbf{L}^T\mathbf{P}_d\mathbf{L}$ is not a

Velocity Stacking Filters

Filter	Offset Range	Kernel $K(p,\tau;\tilde{p},\tilde{\tau})$
$\mathbf{L}^T\mathbf{P}_d\mathbf{L}$	h_1, h_2	$\tilde{\tau}\dfrac{H\left(h_0 - h_1^2\right) H\left(h_2^2 - h_0\right)}{\lvert p^2 - \tilde{p}^2\rvert^{1/2}\lvert \tau^2 - \tilde{\tau}^2\rvert^{1/2}}$
$\mathbf{L}^T\mathbf{L}$	$0, \infty$	$\tilde{\tau}\dfrac{H(h_0)}{\lvert p^2 - \tilde{p}^2\rvert^{1/2}\lvert \tau^2 - \tilde{\tau}^2\rvert^{1/2}}$
$(\mathbf{L}^T\mathbf{P}_d\mathbf{L})^+$	h_1, h_2	$\dfrac{p\tilde{p}\tilde{\tau}}{\pi^2}\dfrac{H\left(h_0 - h_1^2\right) H\left(h_2^2 - h_0\right)}{\lvert p^2 - \tilde{p}^2\rvert^{3/2}\lvert \tau^2 - \tilde{\tau}^2\rvert^{3/2}}$ + edge terms[2]
$(\mathbf{L}^T\mathbf{L})^+$	$0, \infty$	$\dfrac{p\tilde{p}\tilde{\tau}}{\pi^2}\dfrac{H(h_0)}{\lvert p^2 - \tilde{p}^2\rvert^{3/2}\lvert \tau^2 - \tilde{\tau}^2\rvert^{3/2}}$ + edge terms[3]

Notes:

1. $h_0 \equiv -\dfrac{\tau^2 - \tilde{\tau}^2}{p^2 - \tilde{p}^2}$

2. "Edge terms" are the last two terms of equation (4.18) with $x = \tilde{p}^2 - p^2$ and $y = \tilde{\tau}^2 - \tau^2$, multiplied by $16\tilde{p}p\tau$. The kernel is applied using equation (4.21).

3. The edge terms for the infinite aperture filter $(\mathbf{L}^T\mathbf{L})^+$ in the continuous case are infinite and cannot be expressed in terms of deltas or their derivatives. A discrete implementation of the filter (figure 4.1) may use (4.19) to determine these points.

TABLE 4.1. Velocity stacking filters derived in the text.

singular value decomposition; but if $\mathbf{L}^T\mathbf{P}_d\mathbf{L}$ does happen to have a true inverse, it would be uniquely given by

$$(\mathbf{L}^T\mathbf{P}_d\mathbf{L})^{-1} = \mathbf{W}^{-1}\mathbf{S}^{-1}\mathbf{U}\Sigma^{-2}\mathbf{U}^T\mathbf{S} \tag{4.23}$$

Keeping in mind that the inner product in p,τ space is defined with weight τ, we can see that the p^2, τ^2 stretch transformation $\mathbf{S}$ has the Jacobian $4p$:

$$\mathbf{S}^T\mathbf{S} = 4p\mathbf{I}, \qquad \text{therefore } \mathbf{S}^{-1} = \frac{1}{4p}\mathbf{S}^T. \tag{4.24}$$

This fact makes plain the Hermitian nature of $\mathbf{L}^T\mathbf{P}_d\mathbf{L}$:

$$\mathbf{L}^T\mathbf{P}_d\mathbf{L} = \frac{1}{4p}\mathbf{S}^T\mathbf{U}\Sigma^2\mathbf{U}^T\mathbf{S}\frac{1}{4p} \tag{4.25}$$

Recall from chapter 3 that the slant stack pseudoinverse has the singular value decomposition $\mathbf{U}\Sigma^{-2}\mathbf{P}\mathbf{U}^T$; so the generalized inverse of equation (4.25) is

$$(\mathbf{L}^T\mathbf{P}_d\mathbf{L})^+ = \frac{1}{4p}\mathbf{S}^T\mathbf{U}\Sigma^{-2}\mathbf{P}\mathbf{U}^T\mathbf{S}\frac{1}{4p} \tag{4.26}$$

Projection $\mathbf{P}$ represents the Heaviside step functions of equation (4.17). If the system (4.26) is not in the form of a singular value decomposition (i.e., in the form of equation 2.44), then the theorem of section 2.7 does not apply, and it is not clear that we can substitute $(\mathbf{L}^T\mathbf{L})^+$ for $(\mathbf{L}^T\mathbf{P}_d\mathbf{L})^+$ in the generalized inverse solution of $\mathbf{u} = (\mathbf{L}^T\mathbf{P}_d\mathbf{L})^+\mathbf{L}^T\mathbf{P}_d\mathbf{d}$ and thereby expect to get an identical estimate for $\mathbf{u}$. The reason for wanting to do so is strictly one of efficiency: $(\mathbf{L}^T\mathbf{L})^+$ might be easier than $(\mathbf{L}^T\mathbf{P}_d\mathbf{L})^+$ to implement. It happens that it is valid to substitute $(\mathbf{L}^T\mathbf{L})^+$ for $(\mathbf{L}^T\mathbf{P}_d\mathbf{L})^+$; the proof of that validity is outlined below.

As we did in chapter 3, let us examine the analog to the singular value decomposition of $\mathbf{L}^T\mathbf{P}_d$. Equation (2.30) can be put into the form of a slant stack, by remapping the data domain with $\tilde{x} = h^2$, $\tilde{y} = t^2$. Call this mapping $\mathbf{S}_d$. The model domain is mapped into p^2, τ^2 by operator $\mathbf{S}$, which transforms velocity stacking into a slant stacking operation. In integral form, equation $\mathbf{u} = \mathbf{L}^T\mathbf{P}_d\mathbf{d}$ is

$$u(x^{1/2}, y^{1/2}) = \int_0^\infty \frac{d\tilde{x}}{2h} P_d(h)\, d(\tilde{x}^{1/2}, (\tilde{y} = y + x\tilde{x})^{1/2}) \tag{4.27}$$

Or in operator notation, it is

$$\mathbf{u} = \mathbf{S}^{-1}\mathbf{U}\Sigma\mathbf{V}^T\mathbf{S}_d\frac{1}{2h}\mathbf{P}_d\mathbf{d} \tag{4.28}$$

where $\mathbf{V}\Sigma\mathbf{U}^T$ (derived in section 3.3) is the singular value decomposition of the slant stack operator $\mathbf{L}$. Because $\mathbf{P}_d$ is a projection, it commutes with the $1/2h$ multiplier, and is transformed by $\mathbf{S}_d$ into the projection $\mathbf{P}'_d$:

$$P_d'(x) = H(h_2^2 - x)\,H(x - h_1^2)$$

Finally, from section 3.4, $\mathbf{V}^T\mathbf{P'}_d = \mathbf{PV}^T$, where P is in fact identical with the projection of equation (4.26). Because of the commutivity of these various projections, equation (4.28) may be rewritten as

$$\mathbf{u} = \mathbf{L}^T\mathbf{P}_d\mathbf{d} = \mathbf{S}^{-1}\mathbf{U}\Sigma\mathbf{P}\mathbf{V}^T\mathbf{S}_d\frac{1}{2h}\mathbf{d} \tag{4.29}$$

The generalized inverse is the combination of equations (4.26) and (4.29):

$$(\mathbf{L}^T\mathbf{P}_d\mathbf{L})^+\mathbf{L}^T\mathbf{P}_d\mathbf{d} = \left[\frac{1}{4p}\mathbf{S}^T\mathbf{U}\Sigma^{-2}\mathbf{P}\mathbf{U}^T\mathbf{S}\frac{1}{4p}\right]\left[\mathbf{S}^T\mathbf{U}\Sigma\mathbf{P}\mathbf{V}^T\mathbf{S}_d\frac{1}{2h}\mathbf{d}\right] \tag{4.30}$$

or

$$\tilde{\mathbf{u}} = (\mathbf{L}^T\mathbf{P}_d\mathbf{L})^+\mathbf{L}^T\mathbf{P}_d\mathbf{d} = \frac{1}{4p}\mathbf{S}^T\mathbf{U}\Sigma^{-1}\mathbf{P}\mathbf{V}^T\mathbf{S}_d\frac{1}{2h}\mathbf{d} \tag{4.31}$$

The "infinite aperture" version of the generalized inverse is determined from equation (4.26) by inserting the appropriate projection operator $\tilde{\mathbf{P}}$:

$$(\mathbf{L}^T\mathbf{L})^+ = \frac{1}{4p}\mathbf{S}^T\mathbf{U}\Sigma^{-2}\tilde{\mathbf{P}}\mathbf{U}^T\mathbf{S}\frac{1}{4p} \tag{4.32}$$

where $\tilde{P}(\xi,\eta) \equiv H(\xi\eta)$. Because this projection zeros out quadrants II and IV of the Fourier plane, it is clear that $(\mathbf{L}^T\mathbf{L})^+$ may replace $(\mathbf{L}^T\mathbf{P}_d\mathbf{L})^+$ in equation (4.30) without altering the estimate of the inverse $\tilde{\mathbf{u}}$:

$$\tilde{\mathbf{u}} = (\mathbf{L}^T\mathbf{L})^+\mathbf{L}^T\mathbf{P}_d\mathbf{d} = \frac{1}{4p}\mathbf{S}^T\mathbf{U}\Sigma^{-1}\tilde{\mathbf{P}}\mathbf{P}\mathbf{V}^T\mathbf{S}_d\frac{1}{2h}\mathbf{d} \tag{4.33}$$

Recalling that $\tilde{\mathbf{P}}\mathbf{P} = \mathbf{P}$ completes the proof.

It was assumed in this section that $\mathbf{S}^{-1}$ exists. Singular points do occur at $\tau = 0$ and $p = 0$, but if **u** is restricted to a subspace away from this region of the velocity panel, **S** and the other mappings considered here are invertible in practice.

4.5 Synthetic and real data examples

The synthetic gather of figure 4.2 was generated by applying a discrete version of the velocity stacking operator **L**, to a set of four impulses in the velocity plane. The impulses represent reflectors at 1.5, 2.5, 3.5, and 4.5 seconds in a

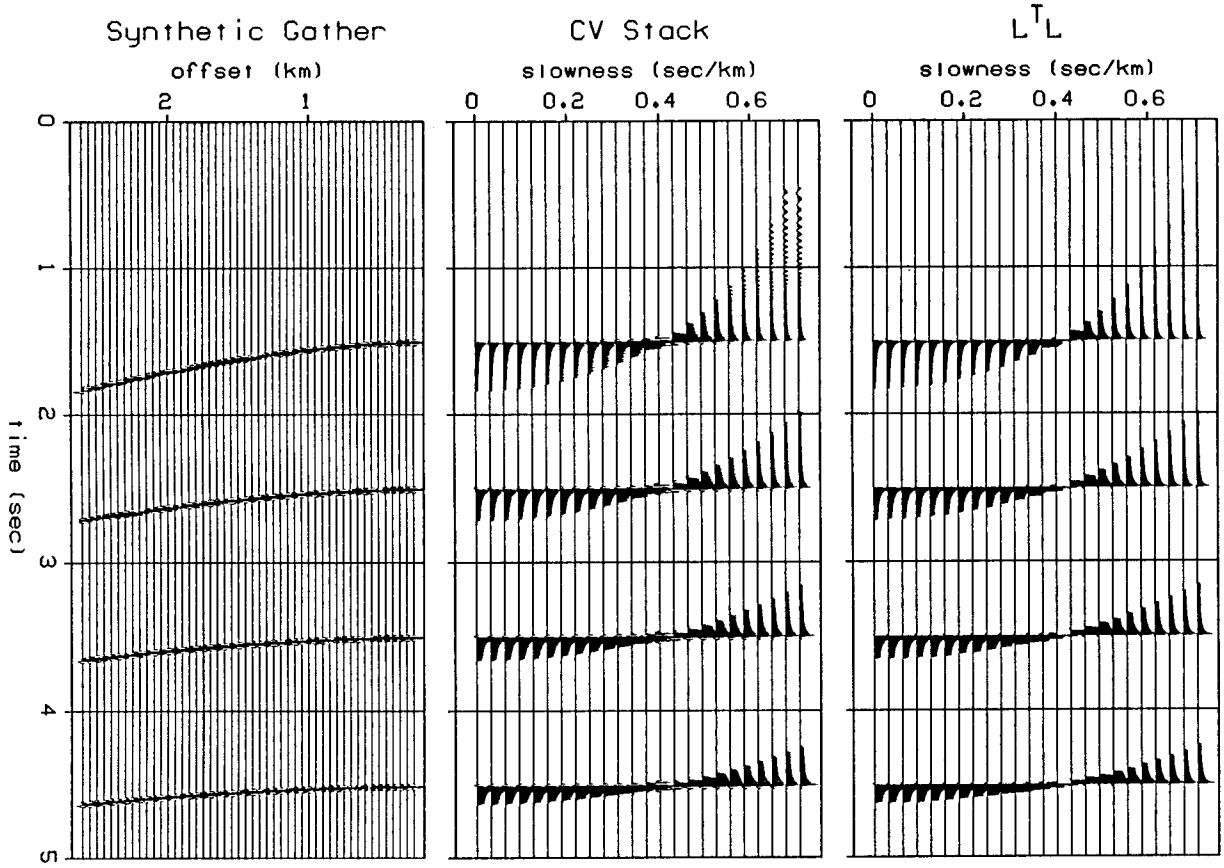

FIG. 4.2. Velocity stack of a synthetic gather. The panel on the left is a simple gather (**d**) with 4 events on it; it was generated by applying **L** to four impulses in the velocity plane that appear between 1.5 and 4.5 seconds, having a slowness of 0.4 seconds/km. The constant velocity stack $\mathbf{L}^T\mathbf{d}$ (center panel) was generated from the synthetic gather. In comparison, the panel on the right was generated by applying $\mathbf{L}^T\mathbf{L}$ of table 4.1 directly to the set of four impulses. The clip value (maximum plotted amplitude) on both velocity stacks is 10% of the maximum amplitude.

medium with a constant velocity of 2500 m/sec. The middle panel of figure 4.2 shows the result of a constant velocity stack applied to the midpoint gather. This panel shows various impulse responses of the discrete version of $\mathbf{L}^T\mathbf{P}_d\mathbf{L}$ at different zero-offset travel times. We may compare the constant velocity stack with the continuous version of the impulse response of $\mathbf{L}^T\mathbf{P}_d\mathbf{L}$ from table 4.1 (rightmost panel of figure 4.2). They are virtually identical. The main difference is the appearance of aliasing artifacts on the discrete impulse response at the shallowest time, 1.5 seconds. The waveform used on the synthetic gather is a truncated sinc function in

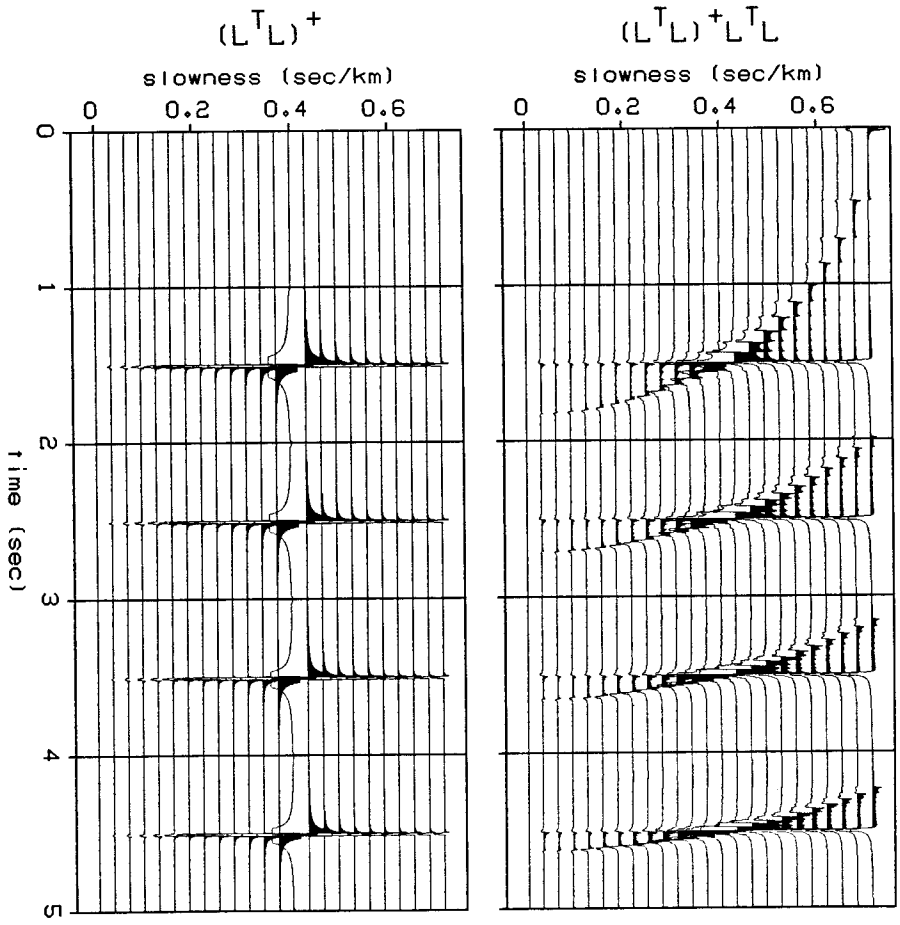

FIG. 4.3. Generalized inverses of synthetic data. The left panel is another display of the impulse response $(L^TL)^+$ shown in figure 4.1; the four impulses of figure 4.2 were used to obtain this response. Clip value of this plot is 1% of the maximum amplitude. The right panel is $(L^TL)^+$ applied to the constant velocity stack of figure 4.2. The clip value of this plot is about 5% of the maximum amplitude.

time. The sidelobes of the sinc function begin to constructively interfere at shallow times and high stacking velocities; thus the sinusoidal nature of the response. The lateral spread (in slowness) of the filter response may be termed the *sidelobes* of velocity stacking. The edge effects from the limitation in offset (the effect of projector $\mathbf{P}_d$) on the synthetic gather are obvious in the constant velocity stack.

The response of $(L^TL)^+$ to the impulses shown in figure 4.2, is presented on the left panel of figure 4.3. These are variable-area plotted versions of the impulse response shown in figure 4.1. The filter $(L^TL)^+$ was designed directly from the

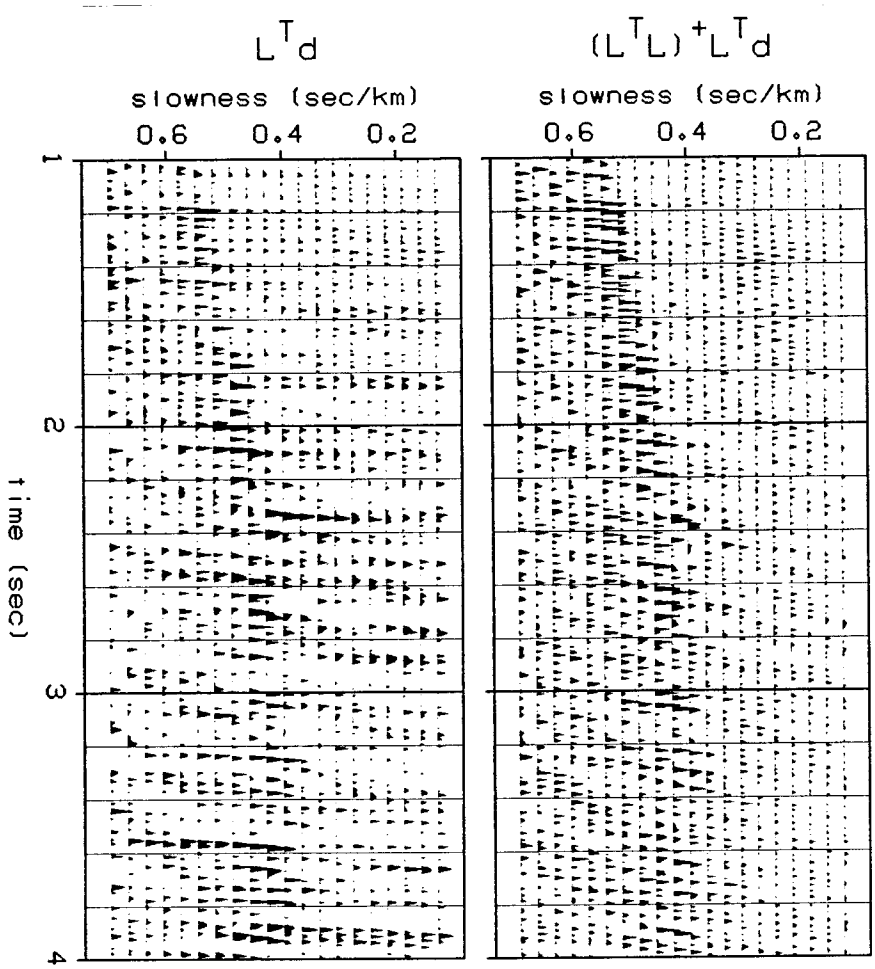

FIG. 4.4. The generalized inverse applied to a common-midpoint gather. $\mathbf{L}^T\mathbf{d}$ is the same velocity stack shown in figure 1.1. By comparison, $(\mathbf{L}^T\mathbf{L})^+\mathbf{L}^T\mathbf{d}$ is the velocity stack filtered with the generalized inverse of table 4.1.

formulas in table 4.1, which satisfy the constraints of equation (4.19). Apart from the p and τ dependent scaling factors, the filter has no DC components in either the p or τ directions. It functions very much like a half-derivative.

The result of applying $(\mathbf{L}^T\mathbf{L})^+$ to the constant velocity stack of figure 4.2 is shown in the right panel of figure 4.3. Because of the differentiation behavior of the generalized inverse, energy in the sidelobes has been reduced; this is the desired effect. It should be noted that the clip amplitude of the variable-area plot of figure 4.3 is approximately one half the clip amplitude of the constant velocity stack in

figure 4.2, so that figure 4.3 is plotted at about twice the scale factor of figure 4.2.

Turning to real data, we apply the generalized inverse to the common-midpoint gather introduced in chapter 1: the data from the Texas Gulf Coast. In figure 4.4 the velocity stack of the data, $\mathbf{L}^T\mathbf{d}$, (also illustrated in figure 1.1) is compared to the velocity stack filtered with the generalized inverse, $(\mathbf{L}^T\mathbf{L})^+\mathbf{L}^T\mathbf{d}$. Figure 1.2 compares the same panels over a smaller time window of 2 to 3 seconds. The lateral resolution of the desired velocity function has been somewhat increased by the rho filtering step.

4.6 Summary: use of the generalized inverse

In chapters 3 and 4, expressions were developed for the generalized inverses of slant stacking and velocity stacking. These filters may be used in two ways: to obtain a better stack, and to obtain an extrapolation of the data by model determination. In the first case, the operator of choice to be applied to the data $\mathbf{d}$ is the generalized inverse $\mathbf{L}^+$ given in equation (4.31). By its use, one attempts to sharpen the image in the velocity panel generated by the forward stack operation $\mathbf{L}^T$. From figure 4.2 it is easy to see how multiple events close in velocity to the desired primaries can contribute significantly to the stack: the sidelobes from the multiple's response will interfere with the focused primary energy. The generalized inverse, by sharpening up the image (suppressing the "sidelobes" of the event) in the velocity domain, helps to separate events of differing velocity.

In the second case, we are able to extrapolate the data once a good velocity panel $\mathbf{L}^+\mathbf{d}$ has been obtained. The velocity panel can then be transformed back into the data domain with a stack operator $\mathbf{L}$ that has a much more finely sampled output space.

4.A Appendix: derivation of $(L^T P_d L)^+$

To derive $(L^T P_d L)^+$ it is necessary to take the inverse Fourier transform of equation (4.17):

$$\tilde{K}^+(x,y) \equiv \frac{1}{4\pi^2}\iint_{-\infty}^{\infty} d\xi\, d\eta\, \frac{|\xi\eta|^{1/2}}{2\pi} H\left(\frac{\xi}{\eta} - h_1^2\right) H\left(h_2^2 - \frac{\xi}{\eta}\right) e^{i\xi x + i\eta y} \quad (4.17)$$

The Fourier transform pair we use is given in equation (3.13). Let us ignore for now the singular point at the origin, and assume that $x \neq 0$ and $y \neq 0$. The integrand is nonzero in the region of the ξ,η plane bounded by the lines $\xi/\eta = h_1^2$ and $\xi/\eta = h_2^2$. To incorporate this region into the integration limits, change the variables of integration to q, r:

$$q \equiv \xi, \quad r \equiv \eta/\xi, \quad d\xi d\eta = |q|\, dq dr$$

so that

$$\tilde{K}^+(x,y) \equiv \frac{1}{8\pi^3}\int_{1/h_2^2}^{1/h_1^2} |r|^{1/2} dr \int_{\infty}^{\infty} q^2 dq\; e^{iq(x+ry)} \quad (4.A1)$$

As a consequence of our symmetric Fourier transform pair, the Dirac delta has the following expression in the transformed domain:

$$\delta''(x) \equiv \frac{d^2}{dx^2}\delta(x) = \frac{1}{\sqrt{2\pi}}\int_{\infty}^{\infty} d\xi \left(\frac{-\xi^2}{\sqrt{2\pi}}\right) e^{i\xi x} \quad (4.A2)$$

Therefore

$$\tilde{K}^+(x,y) \equiv \frac{1}{4\pi^2}\int_{1/h_2^2}^{1/h_1^2} dr\; |r|^{1/2}\delta''(x+ry) \quad (4.A3)$$

There are "edges" to this filter because of the finite limits on the integral. Keeping in mind that the Dirac second derivative represents a limiting sequence of integrable functions, we may integrate by parts:

$$\tilde{K}^+(x,y) = \frac{1}{4\pi^2}\left(I_2 + I_1 + I_0\right) \quad (4.A4)$$

$$I_2 \equiv \left[-|r|^{1/2} \frac{\delta'(x + ry)}{y} \right]_{r = 1/h_2^2}^{1/h_1^2} \tag{4.A5}$$

$$I_1 \equiv \left[\frac{d}{dr}|r|^{1/2} \frac{\delta(x + ry)}{y^2} \right]_{r = 1/h_2^2}^{1/h_1^2} \tag{4.A6}$$

$$I_0 \equiv \int_{1/h_2^2}^{1/h_1^2} -dr \, \frac{d^2}{dr^2}|r|^{1/2} \frac{\delta(x + ry)}{y^2} \tag{4.A7}$$

Now the derivatives of $|r|^{1/2}$ are

$$\frac{d}{dr}|r|^{1/2} = \frac{1}{2}|r|^{-1/2}\,\mathrm{sgn}(r) \tag{4.A8}$$

and

$$\frac{d^2}{dr^2}|r|^{1/2} = -\frac{1}{4}|r|^{-3/2} + |r|^{-1/2}\delta(r) \tag{4.A9}$$

Substituting these expressions into integral I_0 produces

$$I_0 = \int_{1/h_2^2}^{1/h_1^2} dr \left(\frac{1}{4}|r|^{-3/2} \frac{\delta(x/y + r)}{|y|^3} - |r|^{-1/2}\delta(r) \frac{\delta(x + ry)}{y^2} \right) \tag{4.A10}$$

Because $1/h_2^2 > 0$, the second term in the integrand disappears. The delta in the first term constrains the integral to be nonzero only in the region

$$\frac{1}{h_2^2} < -\frac{x}{y} < \frac{1}{h_1^2} \tag{4.A11}$$

Within these limits, the delta sifts the integrand. Using our unit step function notation,

$$I_0 = \frac{1}{4}|xy|^{-3/2} H\left(-\frac{y}{x} - h_1^2\right) H\left(h_2^2 + \frac{y}{x}\right) \tag{4.A12}$$

The integrated parts of equations (4.A5) and (4.A6) are:

$$I_2 = |xy|^{-1/2}\mathrm{sgn}(y)\left(\delta'(y + h_2^2 x) - \delta'(y + h_1^2 x) \right) \tag{4.A13}$$

$$I_1 = -\frac{1}{2}|x|^{-3/2}|y|^{-1/2}\left(\delta(y + h_2^2 x) - \delta(y + h_1^2 x) \right) \tag{4.A14}$$

These three terms, I_o, I_1, I_2 together with equation (4.A4) define the kernel of the pseudoinverse $(\mathbf{L}^T\mathbf{P}_d\mathbf{L})^+$. The formula is summarized in equation (4.18).

The filter coefficient at $x = y = 0$ is needless to say unbounded for the continuous filter. If a discrete version of the filter (4.18) were designed, the constraint that it have zero mean could be used to determine the coefficient at the origin.